



Reductive domino reaction to access chromeno[2,3-*c*]isoquinoline-5-amines with antiproliferative activities against human tumor cells

Xiaoyi Yue^a, Alexey A. Festa^{a,*}, Olga A. Storozhenko^a, Alexey V. Varlamov^a, Karthikeyan Subramani^a, Angelina Boccarelli^b, Rosa Purgatorio^c, Cosimo D. Altomare^{c,*}, Leonid G. Voskressensky^{a,*}

^a Organic Chemistry Department, Science Faculty, Peoples' Friendship University of Russia (RUDN University), Miklukho-Maklaya st., 6, Moscow, Russia

^b Department of Biomedical Sciences and Human Oncology, University of Bari Aldo Moro, Piazza Giulio Cesare 11, 70124 Bari, Italy

^c Department of Pharmacy-Drug Sciences, University of Bari Aldo Moro, Via E. Orabona 4, 70125 Bari, Italy

ARTICLE INFO

Keywords:

Domino reaction
DNA binding
Antiproliferative activity

ABSTRACT

An interaction of homophthalonitrile with salicylaldehydes proceeds as a novel domino reaction and results in the formation of nineteen 12*H*-chromeno[2,3-*c*]isoquinoline-5-amine derivatives. Four new bonds and two cycles are forged in a single synthetic operation, employing cheap and eco-friendly ammonium formate, acting both as a catalyst and a reducing agent. The *in vitro* cytotoxicity tests revealed antiproliferative activities against five human tumor cell lines, including the cisplatin-resistant ovarian carcinoma one (A2780cp8), with inhibitory potency data (IC₅₀) in the low micromolar range in most cases. Molecular docking calculations and fluorescence quenching studies revealed possible binding properties with DNA of the active compounds.

1. Introduction

Domino reactions represent a useful methodology for an effective creation of molecular complexity, especially in the synthesis of polycyclic molecules [1,2]. Fused heterocyclic systems, comprising chromene and pyridine rings are found in versatile compounds with pronounced biological activity. For example, chromenotacrine (e.g., CT6; Fig. 1) may have potential as agents for Alzheimer's disease [3]. Pranoprofen and amlexanox are marketed anti-inflammatory drugs [4,5]. Amlexanox has also shown several pharmacological properties, such as strong anti-tumor effects [6], inhibition of IκB kinase ε (IKKε), TANK binding kinase 1 (TBK1) [7–9] and high-mobility group box 1 (HMGB1) release [10]. Tetracyclic compounds in which the chromene unit is fused with imidazo[1,2-*a*]pyridine proved to be cytotoxic against human colorectal cancer HCT116 cells, inducing cell cycle arrest at G1/G0 phase and apoptosis without significant effects in normal cells [11].

The high impact of spatial planarity of chromenopyridines on bioactivity prompted us to develop a domino route toward the scaffold.

The construction of chromenopyridines usually relies on domino or multicomponent reactions of salicylaldehydes **1** and excess amounts of malononitrile (or malononitrile dimer) [12–17]. We have recently shown that homophthalonitrile **2** works as a vinylogous malononitrile, annulating an isoquinoline ring. The initial formation of the reactive intermediate **A** is followed by the 1,6-addition of a nucleophile to form

the final chromeno[2,3-*c*]isoquinoline-5-amine **3** with nitromethyl- [18], *o*-cyanophenyl-, or indol-3-yl substituents [19] at C(12) (Scheme 1). Following our interest in the domino reactions of cyanomethyl [20–23] or 1,5-dinitrile derivatives [24], herein we report a reductive domino sequence of homophthalonitrile and salicylaldehyde towards annulated isoquinolines. The antiproliferative activities of representative compounds were evaluated *in vitro* against five human tumor cell lines. As suggested in literature for isoquinoline-containing polycyclic compounds with anticancer activity [25–27], the propensity of the tested compounds to DNA binding was also examined through docking calculations and fluorescence spectroscopy studies.

2. Results and discussion

2.1. Synthesis of 12*H*-chromeno[2,3-*c*]isoquinoline-5-amines

Initially, the title product was isolated from the sequential two-step reaction of salicylaldehyde, homophthalonitrile, and 4-*tert*-butylphenol as a nucleophile. It turned out that the phenol acted as a reducing agent, but not a nucleophile (Table 1, Entry 1). Taking into account the importance of the chromenopyridines with a methylene moiety in the pyran ring for the search of biologically active compounds, we got interested in the discovered transformation. The reaction optimization study involved screening of different reducing agents, promoters,

* Corresponding authors.

<https://doi.org/10.1016/j.bioorg.2020.104169>

Received 22 April 2020; Received in revised form 4 July 2020; Accepted 3 August 2020

Available online 28 August 2020

0045-2068/ © 2020 Elsevier Inc. All rights reserved.

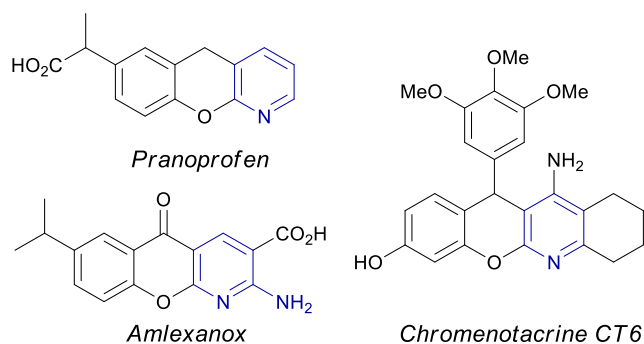
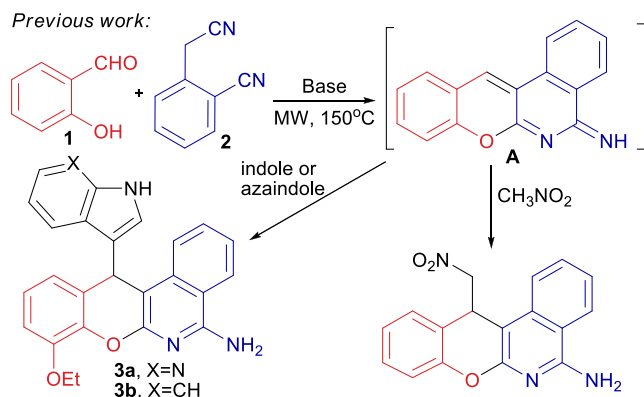


Fig. 1. Representative examples of biologically active chromenopyridines.



Scheme 1. Sequential three component reactions of salicylaldehyde, homophthalonitrile, and nucleophiles.

reagents ratio, and reaction time (Table 1). Firstly, the reactions were performed in a two-step fashion. Homophthalonitrile and salicylaldehyde were irradiated in a microwave reactor for 10 min at 150 °C in the presence of ammonium acetate (2 equiv) to generate the intermediate A. Then, a base and a reducing agent were added to a reaction vessel and heated again at 150 °C for 10 min. The use of hydroquinone (Table 1, Entry 2), formic acid (Table 1, Entry 3), or Hantzsch ester (Table 1, Entry 4) as a reducing agent on a second step led to the isolation of the target product 4a in 53, 65, or 43% yields, respectively. The combination of Hantzsch ester with acidic conditions resulted in a higher 66% yield of 4a (Table 1, Entry 5). To improve the synthetic protocol and avoid two-step procedure, we tried to add formic acid on the first step. We were pleased to isolate the target compound 4a in 39% yield in this case (Table 1, Entry 6). Further, ammonium formate was found to be the reagent of choice due to its possibility to act as both an acid-base catalyst and a reducing agent. Screening the reagents ratio revealed that homophthalonitrile should be taken in 30% excess to produce 4a in 65% yield in a one-step protocol (Table 1, Entries 7–9). The addition of water to a reaction mixture improved the yield of 4a to 75% (Table 1, Entry 10).

The reaction scope was evaluated on different salicylaldehydes. The reductive domino reaction of homophthalonitrile was effective with salicylaldehyde, 5-fluoro and 5-methoxysalicylaldehydes, producing compounds 1a, b, d with good 75–86% yields (Scheme 2). The use of 5-bromo or 5-nitrosalicylaldehydes gave products 1c, e with moderate 48–51% yields. 3-Substituted salicylaldehydes gave ethoxy- and methyl-derivatives 4f and 4g with 73% and 68% yields, respectively. Disubstituted aldehydes were also compatible, and products 4h, i were isolated in 60% and 47% yields, respectively. To evaluate the influence of the substitution in homophthalonitrile moiety on the reaction course, 4-nitrohomophthalonitrile was used. Corresponding compounds 4j–n were synthesized with slightly lesser, but still good 57–67% yields. The reaction of 4-aminohomophthalonitrile led to the formation of complex

mixtures. In its turn, protected 4-acetylaminohomophthalonitrile successfully produced compounds 4o–s in 65–84% yields.

We presume the reaction to proceed through the pathway proposed in Scheme 3. Firstly, the Knoevenagel condensation of homophthalonitrile and salicylaldehyde yields the intermediate B, which undergoes consecutively two nucleophilic cyclizations. Ammonium formate acts as a hydrogen donor, transforming the imine intermediate A into the final amino compound 4.

2.2. Evaluation of the antiproliferative activity

The growth inhibitory effects caused by the chromeno[2,3-c]isoquinoline-5-amine derivatives 4a–i were evaluated toward a panel of human tumor cell lines with different sensitivity to cisplatin (CDDP), used as positive control in the antiproliferative sulforhodamine-B (SRB) test [28]. In addition, two previously reported analogs 3a and 3b, bearing 1H-pyrrolo[2,3-b]pyridin-3-yl and 1H-indol-3-yl moieties, respectively, at C12 of the chromenoisoquinoline scaffold, were also tested for a first evaluation of structure-activity relationships (SARs). The panel of human tumor cells consists of a breast cancer line (MCF-7), a colon (HCT116) and ovarian carcinoma cell lines (SK-OV-3, A2780 and A2780cp8). Ovarian tumor cells are characterized by intrinsic resistance (SK-OV-3) and acquired resistance (A2780cp8) to CDDP [29]. The in vitro inhibitory potencies of the test compounds toward tumor cell growth, expressed as the half-maximal inhibitory concentrations (IC₅₀s), are reported in Table 2.

As shown in the squared correlation matrix (Table 3), the MCF-7 IC₅₀ values were not linearly correlated ($r^2 < 0.50$) with those determined toward the other tested cell lines (Table 4).

In contrast, IC₅₀s determined with colon (HCT116) and ovarian (SK-OV-3, A2780) tumor cell lines resulted well correlated ($r^2 > 0.83$), suggesting that the antiproliferative effects of the chromeno[2,3-c]isoquinoline derivatives toward these three cell lines should be rather similarly affected by the physicochemical properties. Regarding the ovarian carcinoma cells, the IC₅₀s determined with A2780 were highly correlated ($r^2 = 0.95$) with those from the cell line intrinsically resistant to cisplatin (SK-OV-3) and to a lesser extent ($r^2 = 0.80$) with IC₅₀s from the cancer cells with cisplatin acquired resistance (A2780cp8).

As for the human breast cancer cell (MCF-7) growth, compound 4a and its 10-F analog 4b, both equipotent with CDDP, displayed the highest antiproliferative activity. As SAR trend, it appears that the higher the bulkiness/polarizability of the substituents R¹ and R³ the lower the inhibition potency. Some other compounds showed IC₅₀ about or lower than 10 μM (4d, 4f, 4g and 4h). Regarding the 12-substituted compounds, the indol-3-yl moiety in 3b (and not the azaindolyl one in 3a) is tolerated (IC₅₀ equals 11.3 μM, a value close to 14.5 μM that is the IC₅₀ of the parent 4g).

Among the most potent inhibitors of cell growth of HCT116, SK-OV-3 and A2780 cell lines, the 10-methoxy (4d) and 8-ethoxy (4f) analogs attained IC₅₀s in the low micromolar range. Interestingly, in the ovarian cell line A2780, 4d and 4f proved to potently inhibit cell growth with IC₅₀ values of 5.32 and 4.04 μM, respectively.

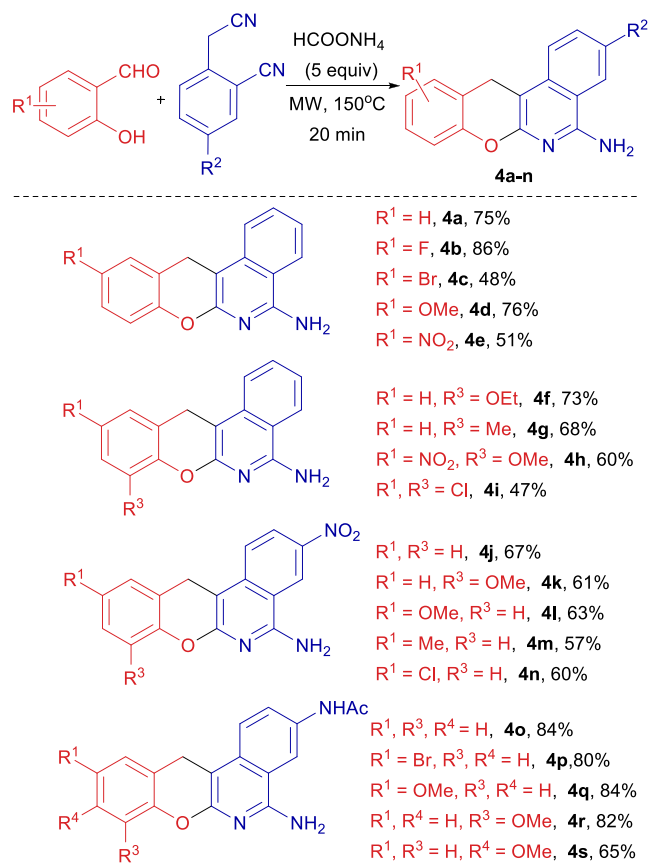
A good antiproliferative activity was retained towards the cisplatin resistant A2780cp8 cells; the resistance factors were 1.8 and 2.4 for 4d and 4f, respectively. The 8-ethoxy compound 4f showed antiproliferative activity not only toward the A2780cp8 line (IC₅₀ = 9.40 μM) characterized by acquired resistance but also toward the SK-OV-3 line (IC₅₀ = 12.5 μM) with intrinsic resistance. Most of the test compounds proved to be able of overcoming the acquired resistance to cisplatin of the ovarian carcinoma A2780cp8 line, which was previously characterized for having higher glutathione content and reduced drug accumulation compared to the parent cell lines [30].

The chromeno[2,3-c]isoquinoline derivatives investigated herein have the typical features of the most common DNA intercalating ligands [31], i.e. a planar polyaromatic moiety bearing a positively charged

Table 1

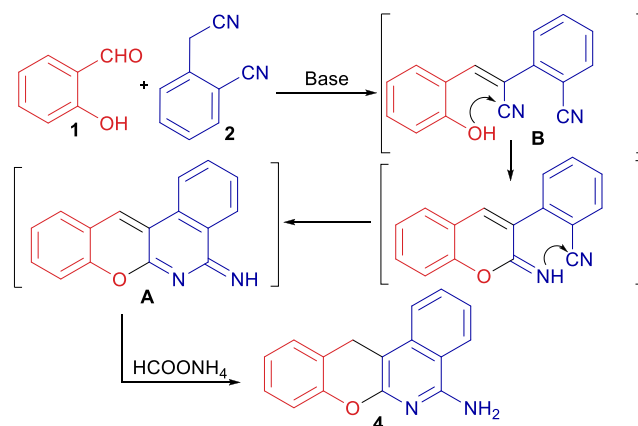
Reaction optimization.

Entry	Ratio 2:1	Solvent	Conditions		Yield, %
			Step 1	Step 2	
1	1:2	<i>i</i> -PrOH	NH ₄ OAc (2 equiv), MW, 150 °C, 10 min	Et ₃ N (1 equiv), 4- <i>tert</i> -butylphenol (2 equiv) MW, 150 °C, 10 min	47
2	1:2	<i>i</i> -PrOH	NH ₄ OAc (2 equiv), MW, 150 °C, 10 min	Et ₃ N (1 equiv), hydroquinone (2 equiv), MW, 150 °C, 10 min	53
3	1:2	<i>i</i> -PrOH	NH ₄ OAc (2 equiv), MW, 150 °C, 10 min	Et ₃ N (1 equiv), Formic acid (2 equiv), MW, 150 °C, 10 min	65
4	1:1.5	<i>i</i> -PrOH	NH ₄ OAc (2 equiv), MW, 150 °C, 10 min	Et ₃ N (1 equiv), Hantzsch ester (2 equiv), MW, 150 °C, 20 min	43
5	1:1.5	<i>i</i> -PrOH	NH ₄ OAc (2 equiv), MW, 150 °C, 10 min	Trifluoroacetic acid (2 equiv), Hantzsch ester (2 equiv), MW, 150 °C, 20 min	66
6	1:1.5	<i>i</i> -PrOH	NH ₄ OAc (2 equiv), Formic acid (5 equiv), MW, 150 °C, 20 min		39
7	1:1.2	<i>i</i> -PrOH	HCOONH ₄ (5 equiv), MW, 150 °C, 20 min		45
8	1.5:1	<i>i</i> -PrOH	HCOONH ₄ (5 equiv), MW, 150 °C, 20 min		54
9	1.3:1	<i>i</i> -PrOH	HCOONH ₄ (5 equiv), MW, 150 °C, 20 min		65
10	1.3:1	<i>i</i> -PrOH-H ₂ O (4:1)	HCOONH ₄ (5 equiv), MW, 150 °C, 20 min		75



Scheme 2. Scope of the reductive domino reaction.

amino group. With a pK_a of ~ 7.6 [28], slightly more than 50% of the 1-aminoisoquinoline group should be protonated at the physiological pH of 7.4. The almost planar tetracyclic system may achieve π - π interactions with two adjacent flanking base pairs (usually CG), whereas the positively charged ammonium group may entropically contribute to stabilize the complex between DNA and the intercalating ligand (i.e. by displacing cations that typically stabilize the DNA structure).



Scheme 3. Proposed reaction pathway.

Table 2

Effects of chromeno[2,3-*c*]isoquinoline-5-amines and cisplatin (CDDP), taken as positive control, on the cell viability of human cancer cell lines, expressed as the concentration for half-maximal inhibition of cell proliferation (IC_{50})^a at 72 h compound exposure.

Cmpd	IC_{50} (μM)					RF ^b
	MCF-7	HCT116	SK-OV-3	A2780	A2780cp8	
4a	1.05	16.6	23.5	11.2	15.1	1.3
4b	1.80	15.7	28.1	9.41	16.4	1.7
4c	23.6	18.5	20.6	10.6	18.7	1.8
4d	7.10	7.90	17.5	5.32	9.71	1.8
4e	24.5	72.0	> 100	78.3	> 100	–
4f	14.5	10.3	12.5	4.04	9.40	2.4
4g	9.50	13.0	27.1	10.0	16.5	1.7
4h	11.7	13.3	53.5	16.5	56.2	3.4
4i	54.2	58.1	> 100	52.5	> 100	–
3a	75.0	74.3	57.3	24.8	81.5	3.3
3b	11.3	13.7	21.8	9.60	14.6	1.5
CDDP	1.50	2.31	3.90	1.55	10.4	6.7

^a Average values of three independent determinations (> 100: < 50% inhibition at 100 μM concentration). Tumor cell lines: MCF-7, human breast carcinoma cell; HCT116, colon cancer cell line; SK-OV-3, human ovarian carcinoma with intrinsic resistance to cisplatin; A2780, human ovarian carcinoma cell; A2780cp8, human ovarian carcinoma with acquired resistance to cisplatin. ^b Resistance factor: $IC_{50}A2780cp8/IC_{50}A2780$.

Table 3
Squared correlation matrix (r^2) of the antiproliferative activities as expressed by $-\log IC_{50}$ values against the tested human cancer cell lines.

	MCF-7	HCT116	SK-OV-3	A2780	A2780cp8
MCF-7	1				
HCT116	0.494	1			
SKOV-3	0.392	0.831	1		
A2780	0.383	0.877	0.947	1	
A2780 cp8	0.445	0.700	0.774	0.802	1

Table 4
Docking score and Glide energy of DNA complexed with compounds 4a, 4d, 4f and 4i.

Cmpd	Docking score (kcal/mol)	Glide energy (kcal/mol)
4a	-7.81	-40.84
4d	-8.64	-47.02
4f	-8.15	-44.70
4i	-8.09	-42.65

2.3. Assessment of propensity targeting DNA

To examine whether the tested compounds may bind DNA through intercalation, molecular docking calculations, combined with preliminary experimental fluorescence spectroscopic studies, were performed with some representative active compounds.

In-silico methods, including molecular docking calculations, might provide us with good explanatory and predictive results [32]. In this study, a molecular docking analysis was carried out to detect a plausible binding interactions and to calculate the energetics of the complexes between DNA (PDB ID: 1BNA) and compounds 4a, 4d, 4f and 4i, using the Standard Precision (SP) method of Glide from Schrödinger v. 2018-2 [33].

Fig. 2 shows the best ranked docking poses of the examined ligands. All the tetracyclic planar chromeno[2,3-c]isoquinoline systems interact between the adjacent DNA base pairs, thereby indicating that the tested compounds may achieve the binding mode into the DNA major groove. Docking scores and Glide energies in Table 3 show that 4d and 4f,

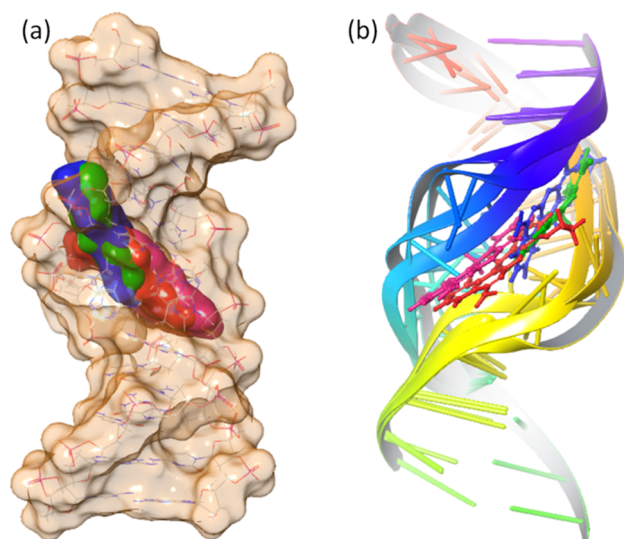


Fig. 2. The highest-scored Glide docking poses of compounds 4a (pink), 4d (blue), 4f (red) and 4i (green) into the major groove of the DNA double-strand fragment (PDB ID: 1BNA); (a) surface representation and (b) cartoon representation of the DNA complex with the intercalating ligands. (For interpretation of the references to colour in this figure legend, the reader is referred to the web version of this article.)

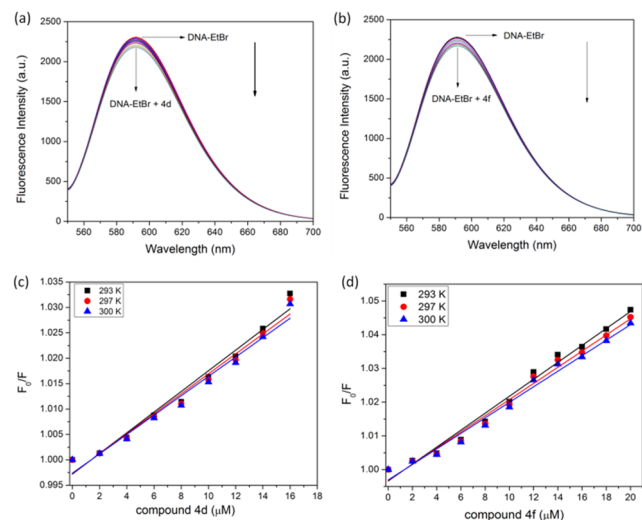


Fig. 3. The emission spectra (a and b) and Stern-Volmer plots at three temperatures (c and d) of ctDNA-EtBr complex upon addition of compounds 4d and 4f, respectively, from 0 to 20 μM (2 μM increasing addition).

compared with 4a and 4i, may achieve slightly stronger interactions with DNA counterparts, which is in accordance with their anti-proliferative activity, evaluated in all the tested cell lines and in particular in the ovarian lines SK-OV-3, A2780 and A2780cp8. Interestingly, looking at the ligands' plot of the best binding poses into the DNA complexes (Fig. S1 in Supporting Information), besides the $\pi-\pi$ interactions, only with for 4d and 4f the 5-NH₂ group may form additional stabilizing H-bond contacts with thymine (DT8) and cytosine (DC9), respectively, in the flanking DNA base pairs.

The potential of 4d and 4f in binding into DNA were further investigated through fluorescence quenching studies of the interaction of the test compounds with calf thymus DNA (ctDNA) complexed with ethidium bromide (EtBr). DNA has low fluorescence intensity. EtBr dye, which binds specifically between the adjacent DNA base pairs, was used to enhance the intensity of DNA complex system. In principle, compounds which compete with EtBr in intercalating DNA affect the DNA-EtBr fluorescence intensity maximum [34].

As shown in Fig. 3, the emission spectrum of ctDNA-EtBr complex changed in the presence of varying amounts of compounds 4d and 4f (Fig. 3, a and b). As the concentration of the added test compound increases, the emission spectral maximum of the ctDNA-EtBr complex decreases. This indicates that in ctDNA-EtBr environment, without any further shift, there is an intercalation possibility for both compounds 4d and 4f, due its competitiveness in ctDNA-EtBr complex system.

In addition, the quenching mechanism and binding constants were determined, using Stern-Volmer and double logarithmic plots (Fig. 3 c-d; Fig. S5 a-b); the calculated values are reported in Table ST1 (Supp. Info.). Quenching mechanism can be classified as static mode and dynamic mode and the average scatter collision limit, defined as $k_q = 2.0 \times 10^{10} \text{ L mol}^{-1} \text{ s}^{-1}$. If the k_q value is above the average k_q , then it refers to the static quenching mode and the calculated values of k_q for compounds 4d and 4f shows that quenching can be a static mode. The binding constant (K_b) and binding site (n) calculations showed good linearity in the ctDNA-EtBr system, which indicates that there is possibility of noncovalent intercalation between both compounds 4d and 4f in the ctDNA-EtBr complex system. In addition, the thermal parameters of enthalpy (ΔH°), entropy (ΔS°) and binding free energy (ΔG°) were also calculated for 4d and 4f with ctDNA-EtBr complex system at three different temperatures (293 K, 297 K, 300 K) using von't Hoff plots (Fig. S5c-d and Table ST2 in Supp. Info.). According to Ross, Subramanian et al. [35], both enthalpy (ΔH°) and entropy (ΔS°) showed positive values, suggesting that binding of 4d and 4f into the ctDNA-EtBr system might be hydrophobic in nature.

2.4. Experimental

Solvents were distilled and dried according to standard procedures. ^1H and ^{13}C NMR spectra were acquired on 400 or 600 MHz spectrometers and referenced to the residual signals of the solvent (for ^1H and ^{13}C). The solvents used for NMR were DMSO- d_6 . Chemical shifts are reported in parts per million (δ /ppm). Coupling constants are reported in Hertz (J/Hz). The peak patterns are indicated as follows: s, singlet; d, doublet; t, triplet; q, quadruplet; m, multiplet; dd, doublet of doublets and br s, broad singlet. Infrared spectra were measured on a FT/IR instrument. The wavenumbers are reported in reciprocal centimeters (ν_{max} /cm $^{-1}$). HRMS spectra were recorded on Bruker MicrOTOF-Q II. MW-assisted reactions were carried out in a Monowave 300 MW reactor from Anton Paar GmbH; the reaction temperature was monitored by an IR sensor. Standard 10 mL G10 reaction vials, sealed with silicone septa, were used for the MW irradiation experiments. The reaction progress was monitored by TLC and the spots were visualized under UV light (254 or 365 nm). Column chromatography was performed using silica gel (230–400 mesh), mixtures of hexane with ethyl acetate used as a mobile phase. Melting points were determined on a SMP-10 apparatus.

2.5. Synthesis of 12,12-dihydrochromenoisoquinoline-5-amines 4a-4q (general procedure)

A solution of homophthalonitrile (185 mg, 1.3 mmol) and salicylaldehyde (122 mg, 1 mmol) in *i*-PrOH-H $_2$ O (3.2 mL-0.8 mL) was treated with HCOONH $_4$ (315 mg, 5 mmol). The reaction mixture was placed into a microwave reactor and heated at 150 °C for 20 min. When the reaction was finished, the solvent was evaporated at reduced pressure. The residual solid was chromatographed over silica gel, eluting with 20%-50% ethyl acetate in hexane solution.

2.5.1. 12,12-Dihydrochromeno[2,3-*c*]isoquinolin-5-amine (4a)

Pale yellow solid, yield 186 mg (75%); m.p. 143–145 °C; ^1H NMR (DMSO- d_6 , 600 MHz): 4.14 (2H, s), 7.02 (2H, s), 7.05–7.13 (2H, m), 7.24 (1H, t, J = 7.1 Hz), 7.35 (1H, d, J = 7.6 Hz), 7.36–7.41 (1H, m), 7.69 (2H, d, J = 3.5 Hz), 8.23 (1H, d, J = 8.1 Hz); ^{13}C NMR (DMSO- d_6 , 150 MHz): δ_{C} ppm = 24.4, 91.4, 116.0, 116.8, 120.5, 122.3, 123.7, 123.7, 125.1, 128.2, 130.0, 131.1, 138.0, 151.5, 152.8, 157.0. HRMS (TOF ES $^+$): m/z calcd for C $_{16}$ H $_{13}$ N $_2$ O [(M+H) $^+$] 249.1022; found 249.1029; IR (KBr): 3306 (NH $_2$).

2.5.2. 12,12-Dihydro-10-fluorochromeno[2,3-*c*]isoquinolin-5-amine (4b)

Pale yellow solid, yield 230 mg (86%); m.p. 140–142 °C; ^1H NMR (DMSO- d_6 , 600 MHz): 4.14 (2H, s), 7.04 (2H, s), 7.06–7.13 (2H, m), 7.19 (1H, t, J = 8.4 Hz), 7.39 (1H, t, J = 7.3 Hz), 7.62–7.67 (1H, m), 7.69 (1H, t, J = 7.3 Hz), 8.22 (1H, d, J = 8.4 Hz); ^{13}C NMR (DMSO- d_6 , 150 MHz): δ_{C} ppm = 24.6, 90.4, 114.86, 115.0, 115.9, 118.3, 122.2, 123.8, 125.1, 131.2, 137.8, 147.8, 152.7, 157.0, 157.5, 159.0. HRMS (TOF ES $^+$): m/z calcd for C $_{16}$ H $_{12}$ FN $_2$ O [(M+H) $^+$] 267.0928; found 267.0935; IR (KBr): 3283 (NH $_2$).

2.5.3. 12,12-Dihydro-10-bromochromeno[2,3-*c*]isoquinolin-5-amine (4c)

Yellow solid, yield 158 mg (48%); m.p. 137–138 °C; ^1H NMR (DMSO- d_6 , 600 MHz): 4.14 (2H, s), 7.03 (1H, s), 7.05 (2H, s), 7.40 (2H, d, J = 8.1 Hz), 7.54 (1H, s), 7.65–7.69 (2H, m), 8.22 (1H, d, J = 8.1 Hz); ^{13}C NMR (DMSO- d_6 , 150 MHz): δ_{C} ppm = 24.2, 90.8, 115.0, 116.1, 119.1, 122.3, 123.4, 123.9, 125.1, 130.9, 131.2, 132.3, 137.8, 150.9, 152.4, 157.0; HRMS (TOF ES $^+$): m/z calcd for C $_{16}$ H $_{12}$ BrN $_2$ O [(M+H) $^+$] 327.0128; found 329.0136; IR (KBr): 3310 (NH $_2$).

2.5.4. 12,12-Dihydro-10-methoxychromeno[2,3-*c*]isoquinolin-5-amine (4d)

Yellow solid, yield 212 mg (76%); m.p. 139 °C; ^1H NMR (DMSO- d_6 , 600 MHz): 3.75 (3H, s), 4.12 (2H, s), 6.82 (1H, dd, J = 8.8, 2.6 Hz), 6.91 (1H, d, J = 2.5 Hz), 6.95–7.04 (3H, m), 7.38 (1H, t, J = 8.1 Hz), 7.62–7.73 (2H, m), 8.21 (1H, d, J = 8.6 Hz); ^{13}C NMR (DMSO- d_6 , 150 MHz): δ_{C} ppm = 24.8, 55.9, 90.8, 114.0, 114.1, 115.9, 117.6, 121.2, 122.16, 123.6, 125.1, 131.1, 138.0, 145.4, 153.0, 155.5, 156.9; HRMS (TOF ES $^+$): m/z calcd for C $_{17}$ H $_{15}$ N $_2$ O $_2$ [(M+H) $^+$] 279.1128; found 279.1133; IR (KBr): 3300 (NH $_2$).

2.5.5. 12,12-Dihydro-10-nitrochromeno[2,3-*c*]isoquinolin-5-amine (4e)

Orange solid, yield 150 mg (51%); m.p. 162–163 °C; ^1H NMR (DMSO- d_6 , 600 MHz): 4.28 (2H, s), 7.14 (2H, s), 7.29 (1H, d, J = 9.1 Hz), 7.44 (1H, t, J = 7.6 Hz), 7.67–7.71 (1H, m), 7.74 (1H, t, J = 7.6 Hz), 8.14 (1H, dd, J = 9.1 Hz, 2.5 Hz), 8.25 (1H, d, J = 8.1 Hz), 8.30 (1H, d, J = 2.5 Hz); ^{13}C NMR (DMSO- d_6 , 150 MHz): δ_{C} ppm = 24.2, 90.8, 116.4, 118.0, 122.2, 122.4, 124.2, 124.4, 125.2, 126.0, 131.4, 137.6, 143.2, 151.9, 156.7, 157.2; HRMS (TOF ES $^+$): m/z calcd for C $_{16}$ H $_{12}$ N $_3$ O $_3$ [(M+H) $^+$] 294.0873; found 294.0878; IR (KBr): 3297 (NH $_2$).

2.5.6. 12,12-Dihydro-8-ethoxychromeno[2,3-*c*]isoquinolin-5-amine (4f)

Pale yellow solid, yield 214 mg (73%); m.p. 151–152 °C; ^1H NMR (DMSO- d_6 , 600 MHz): 1.39 (3H, t, J = 7.1 Hz), 4.07 (2H, d, J = 6.9 Hz), 4.12 (2H, s), 6.86–6.92 (2H, m), 6.99 (1H, t, J = 7.8 Hz), 7.02 (2H, s), 7.33–7.44 (1H, m), 7.68 (2H, d, J = 4.0 Hz), 8.21 (1H, d, J = 8.1 Hz); ^{13}C NMR (DMSO- d_6 , 150 MHz): δ_{C} ppm = 15.3, 24.5, 64.4, 91.2, 111.9, 116.0, 121.2, 122.3, 123.4, 123.4, 123.7, 125.1, 131.1, 137.9, 141.1, 147.4, 152.7, 156.9; HRMS (TOF ES $^+$): m/z calcd for C $_{18}$ H $_{17}$ N $_2$ O $_2$ [(M+H) $^+$] 293.1284; found 293.1293; IR (KBr): 3300 (NH $_2$).

2.5.7. 12,12-Dihydro-8-methylchromeno[2,3-*c*]isoquinolin-5-amine (4g)

Yellow solid, yield 179 mg (68%); m.p. 144 °C; ^1H NMR (DMSO- d_6 , 600 MHz): 2.30 (3H, s), 4.13 (2H, s), 6.98 (1H, t, J = 7.6 Hz), 7.03–7.13 (3H, m), 7.16 (1H, d, J = 7.6 Hz), 7.39 (1H, dd, J = 8.1 Hz, 4.0 Hz), 7.69 (2H, d, J = 3.5 Hz), 7.69 (1H, d, J = 8.1 Hz); ^{13}C NMR (DMSO- d_6 , 150 MHz): δ_{C} ppm = 16.3, 24.5, 91.4, 116.0, 120.0, 122.3, 123.2, 123.7, 125.1, 125.4, 127.5, 129.3, 131.1, 138.0, 149.7, 152.8, 157.0; HRMS (TOF ES $^+$): m/z calcd for C $_{17}$ H $_{15}$ N $_2$ O [(M+H) $^+$] 263.1179; found 263.1185; IR (KBr): 3283 (NH $_2$).

2.5.8. 12,12-Dihydro-8-methoxy-10-nitrochromeno[2,3-*c*]isoquinolin-5-amine (4h)

Brown solid, yield 194 mg (60%); m.p. 167 °C; ^1H NMR (DMSO- d_6 , 600 MHz): 3.97 (3H, s), 4.25 (2H, s), 7.10 (2H, s), 7.43 (1H, t, J = 7.6 Hz), 7.67–7.74 (3H, m), 7.91 (1H, s), 8.23 (1H, d, J = 8.6 Hz); ^{13}C NMR (DMSO- d_6 , 150 MHz): δ_{C} ppm = 24.4, 56.9, 90.7, 105.8, 116.4, 117.6, 121.9, 122.4, 124.3, 125.1, 131.3, 137.6, 142.8, 146.5, 148.4, 151.9, 157.1; HRMS (TOF ES $^+$): m/z calcd for C $_{17}$ H $_{14}$ N $_3$ O $_4$ [(M+H) $^+$] 324.0979; found 324.0986; IR (KBr): 3287 (NH $_2$).

2.5.9. 12,12-Dihydro-8,10-dichlorochromeno[2,3-*c*]isoquinolin-5-amine (4i)

Pale yellow solid, yield 149 mg (47%); m.p. 146 °C; ^1H NMR (DMSO- d_6 , 600 MHz): 4.19 (2H, s), 7.17 (2H, s), 7.41–7.44 (2H, m), 7.54 (1H, d, J = 2.0 Hz), 7.65 (1H, d, J = 8.3 Hz), 7.71 (1H, d, J = 7.5 Hz), 8.23 (1H, d, J = 8.3 Hz); ^{13}C NMR (DMSO- d_6 , 150 MHz): δ_{C} ppm = 24.6, 90.8, 116.4, 121.9, 122.4, 124.2, 124.5, 125.2, 127.0, 128.0, 128.4, 131.3, 137.6, 146.5, 152.1, 157.2; HRMS (TOF ES $^+$): m/z calcd for C $_{16}$ H $_{11}$ Cl $_2$ N $_2$ O [(M+H) $^+$] 318.0321; found, 318.0325; IR (KBr): 3279 (NH $_2$).

2.5.10. 12,12-Dihydro-3-nitrochromeno[2,3-*c*]isoquinolin-5-amine (**4j**)

Orange solid, yield 196 mg (67%); m.p. 245–246 °C; ¹H NMR (DMSO-*d*₆, 600 MHz): 4.17 (2H, s), 7.09–7.15 (2H, m), 7.27 (1H, t, *J* = 7.1 Hz), 7.36 (1H, d, *J* = 7.1 Hz), 7.67 (2H, s), 7.83 (1H, dd, *J* = 9.1, 2.0 Hz), 8.38 (1H, dd, *J* = 9.1, 2.0 Hz), 9.29 (1H, s); ¹³C NMR (DMSO-*d*₆, 150 MHz): δ_C ppm = 24.3, 92.6, 114.4, 116.9, 120.3, 122.6, 123.8, 124.4, 124.5, 128.4, 130.0, 141.7, 143.0, 151.0, 156.4, 158.8. HRMS (TOF ES⁺): *m/z* calcd for C₁₆H₁₂N₃O₃ [(M+H)⁺] 294.0873; found 294.0869; IR (KBr): 1572(NO₂), 3183 (NH₂).

2.5.11. 12,12-Dihydro-8-methoxy-3-nitrochromeno[2,3-*c*]isoquinolin-5-amine (**4k**)

Brown solid, yield 197 mg (61%), m.p. 235 °C; ¹H NMR (DMSO-*d*₆, 600 MHz): 3.83 (3H, s), 4.07 (2H, s), 6.86 (1H, d, *J* = 7.6 Hz), 6.9 (1H, d, *J* = 8.1 Hz), 7.02 (1H, t, *J* = 8.1 Hz), 7.60 (2H, s), 7.73 (1H, d, *J* = 9.1 Hz), 8.31(1H, d, *J* = 7.1 Hz), 9.23(1H, d, *J* = 2.5 Hz); ¹³C NMR (DMSO-*d*₆, 150 MHz): δ_C ppm = 24.3, 56.3, 92.4, 111.1, 114.4, 120.8, 121.1, 122.5, 123.6, 123.9, 124.3, 140.4, 141.6, 142.9, 148.2, 156.3, 158.7; HRMS (TOF ES⁺): *m/z* calcd for C₁₇H₁₄N₃O₄ [(M+H)⁺] 324.0979; found 324.0985; IR (KBr): 1569 (NO₂), 3166 (NH₂).

2.5.12. 12,12-Dihydro-10-methoxy-3-nitrochromeno[2,3-*c*]isoquinolin-5-amine (**4l**)

Orange solid, yield 204 mg (63%), m.p. 137–138 °C; ¹H NMR (DMSO-*d*₆, 600 MHz): 3.76 (3H, s), 4.13 (2H, s), 6.83–6.85 (1H, m), 6.90 (1H, d, *J* = 2.7 Hz), 7.04 (1H, d, *J* = 9.1 Hz), 7.62 (2H, s), 7.77 (1H, d, *J* = 9.1 Hz), 8.36–8.38 (1H, m), 9.27 (1H, d, *J* = 2.4 Hz); ¹³C NMR (DMSO-*d*₆, 150 MHz): δ_C ppm = 24.9, 56.0, 92.1, 114.0, 114.2, 114.3, 117.8, 121.0, 122.7, 123.6, 124.5, 141.7, 142.9, 144.8, 155.9, 156.7, 158.7; HRMS (TOF ES⁺): *m/z* calcd for C₁₇H₁₄N₃O₄ [(M+H)⁺] 324.0979; found 324.0979; found 325; IR (KBr): 1573 (NO₂), 3164 (NH₂).

2.5.13. 12,12-Dihydro-10-methyl-3-nitrochromeno[2,3-*c*]isoquinolin-5-amine (**4m**)

Orange solid, yield 175 mg (57%), m.p. 224 °C; ¹H NMR (CDCl₃, 600 MHz): 2.28 (3H, s), 4.09 (2H, s), 6.95 (2H, m), 7.04 (1H, d, *J* = 8.6 Hz), 7.14 (1H, s), 7.36–7.39 (1H, m), 7.68 (2H, m), 8.21 (1H, d, *J* = 8.1 Hz); ¹³C NMR (CDCl₃, 150 MHz): δ_C ppm = 20.8, 24.4, 91.3, 116.0, 116.6, 120.1, 122.2, 123.6, 125.1, 128.7, 130.1, 131.1, 132.6, 138.0, 149.4, 152.9, 156.9; HRMS (TOF ES⁺): *m/z* calcd for C₁₇H₁₄N₃O₃ [(M+H)⁺] 308.1030; found 308.1022; IR (KBr): 1573 (NO₂), 3164 (NH₂).

2.5.14. 12,12-Dihydro-10-chloro-3-nitrochromeno[2,3-*c*]isoquinolin-5-amine (**4n**)

Pale brown solid, yield 197 mg (60%), m.p. 240–241 °C; ¹H NMR (DMSO-*d*₆, 600 MHz): 5.51 (2H, s), 7.24 (1H, t, *J* = 7.1 Hz), 7.34–7.41 (3H, m), 7.47 (1H, t, *J* = 7.6 Hz), 7.54 (1H, s), 8.74 (1H, d, *J* = 8.1 Hz), 7.81 (1H, d, *J* = 8.6 Hz); ¹³C NMR (DMSO-*d*₆, 150 MHz): δ_C ppm = 35.5, 84.3, 85.0, 109.2, 111.7, 113.8, 115.1, 121.9, 122.2, 122.9, 126.3, 126.7, 129.3, 129.6, 132.0, 137.6; HRMS (TOF ES⁺): *m/z* calcd for C₁₆H₁₁ClN₃O₃ [(M+H)⁺] 328.0483; found 328.0484; IR (KBr): 1573 (NO₂), 3164 (NH₂).

2.5.15. 3-Acetylamino-12,12-dihydrochromeno[2,3-*c*]isoquinolin-5-amine (**4o**)

Yellow solid, yield 276 mg (84%); m.p. 144–145 °C; ¹H NMR (DMSO-*d*₆, 600 MHz): 2.09 (3H, s), 4.14 (2H, s), 6.77 (2H, s), 7.07 (2H, m), 7.24 (1H, t, *J* = 7.6 Hz), 7.34 (1H, d, *J* = 7.6 Hz), 7.66 (1H, d, *J* = 8.6 Hz), 7.68 (1H, d, *J* = 8.6 Hz), 8.31 (1H, s), 10.40 (1H, s); ¹³C NMR (DMSO-*d*₆, 150 MHz): δ_C ppm = 24.3, 24.4, 91.6, 114.7, 116.3, 116.8, 120.5, 122.7, 123.7, 125.3, 128.1, 130.0, 134.3, 135.4, 151.6, 151.9, 156.4, 168.9. HRMS (TOF ES⁺): *m/z* calcd for C₁₈H₁₆N₃O₂ [(M+H)⁺] 306.1237; found 306.1238; IR (KBr): 1593 (C=O), 3175 (NH), 3330 (NH₂).

2.5.16. 3-Acetylamino-12,12-dihydro-10-bromochromeno[2,3-*c*]isoquinolin-5-amine (**4p**)

Yellow solid, yield 236 mg (80%), m.p. 170–172 °C; ¹H NMR (DMSO-*d*₆, 600 MHz): 2.09 (3H, s), 4.14 (2H, s), 6.79 (2H, s), 7.09 (1H, d, *J* = 8.6 Hz), 7.28 (1H, dd, *J* = 8.5, 2.5 Hz), 7.40 (1H, s), 7.61 (1H, d, *J* = 9.1 Hz), 7.83 (1H, d, *J* = 9.1 Hz), 8.33(1H, s), 10.24 (1H, s); ¹³C NMR (DMSO-*d*₆, 150 MHz): δ_C ppm = 24.3, 26.0, 62.6, 91.0, 114.8, 118.6, 122.7, 122.8, 125.5, 127.1, 128.0, 129.4, 134.2, 135.4, 150.5, 151.7, 156.5, 166.0; HRMS (TOF ES⁺): *m/z* calcd for C₁₈H₁₅BrN₃O₂ [(M+H)⁺] 384.0342; found 384.0346; IR (KBr): 1626 (C=O), 3175 (NH), 3330 (NH₂).

2.5.17. 3-Acetylamino-12,12-dihydro-10-methoxychromeno[2,3-*c*]isoquinolin-5-amine (**4q**)

Yellow solid, yield 217 mg (84%), m.p. 152–154 °C; ¹H NMR (DMSO-*d*₆, 600 MHz): 2.09 (3H, s), 3.75 (3H, s), 4.11 (2H, s), 6.73 (2H, s), 6.81 (1H, dd, *J* = 8.1 Hz, 3.0 Hz), 6.89 (1H, d, *J* = 3.0 Hz), 7.00 (1H, d, *J* = 8.6 Hz), 7.62 (1H, d, *J* = 8.6 Hz), 7.84 (1H, d, *J* = 8.1 Hz), 8.33 (1H, s), 10.40 (1H, s); ¹³C NMR (DMSO-*d*₆, 150 MHz): δ_C ppm = 24.3, 24.8, 55.9, 91.0, 114.0, 114.1, 116.2, 117.6, 121.1, 122.6, 125.4, 133.4, 135.2, 145.5, 152.1, 155.5, 156.4, 166.1, 168.8; HRMS (TOF ES⁺): *m/z* calcd for C₁₉H₁₈N₃O₃ [(M+H)⁺] 336.1343; found 336.1341; IR (KBr): 1625 (C=O), 3171 (NH), 3299 (NH₂).

2.5.18. 3-Acetylamino-12,12-dihydro-8-methoxychromeno[2,3-*c*]isoquinolin-5-amine (**4r**)

Yellow solid, yield 212 mg (82%), m.p. 165–166 °C; ¹H NMR (DMSO-*d*₆, 600 MHz): 2.09 (3H, s), 3.83 (3H, s), 4.12 (2H, s), 6.73 (2H, s), 6.90 (2H, m), 7.00 (1H, t, *J* = 7.6 Hz), 7.65 (1H, d, *J* = 9.1 Hz), 7.80 (1H, d, *J* = 8.6 Hz), 8.31 (1H, s), 10.20 (1H, s); ¹³C NMR (DMSO-*d*₆, 150 MHz): δ_C ppm = 24.3, 24.5, 56.3, 91.5, 111.0, 114.7, 116.3, 121.1, 121.3, 122.8, 123.3, 125.4, 134.4, 135.2, 141.1, 148.2, 151.9, 156.3, 168.8; HRMS (TOF ES⁺): *m/z* calcd for C₁₉H₁₈N₃O₃ [(M+H)⁺] 336.1343; found 336.1336; IR (KBr): 1631 (C=O), 3175 (NH), 3278 (NH₂).

2.5.19. 3-Acetylamino-12,12-dihydro-9-methoxychromeno[2,3-*c*]isoquinolin-5-amine (**4s**)

Yellow solid, yield 168 mg (65%), m.p. 136 °C; ¹H NMR (DMSO-*d*₆, 600 MHz): 2.09 (3H, s), 3.40 (3H, s), 4.15 (2H, s), 6.78 (2H, s), 7.04 (1H, d, *J* = 8.6 Hz), 7.40 (1H, dd, *J* = 8.1, 2.0 Hz), 7.53 (1H, d, *J* = 2.0 Hz), 7.62 (1H, d, *J* = 9.1 Hz), 7.78 (1H, d, *J* = 8.1 Hz), 8.28 (1H, s), 10.11 (1H, s); ¹³C NMR (DMSO-*d*₆, 150 MHz): δ_C ppm = 24.2, 26.0, 62.6, 91.1, 114.8, 114.9, 116.4, 119.1, 122.8, 123.3, 125.6, 130.9, 132.3, 134.3, 135.3, 151.0, 151.6, 156.5, 168.8; HRMS (TOF ES⁺): *m/z* calcd for C₁₉H₁₈N₃O₃ [(M+H)⁺] 336.1343; found 336.1342; IR (KBr): 1698 (C=O), 3112 (NH), 3329 (NH₂).

2.6. Cell lines

Human cell lines representative of breast (MCF7), colon (HCT-116), and ovarian (SK-OV-3) cancer were obtained from the National Cancer Institute, Biological Testing Branch (Frederick, MD, USA). The cells were maintained in the logarithmic phase and incubated at 37 °C under a 5% CO₂ humidified air in RPMI 1640 medium supplemented with 10% fetal calf serum, 2 mM glutamine, penicillin and streptomycin (100 U/mL and 0.1 mg/mL, respectively). Instead, A2780/A2780cp8, human ovarian cancer cell lines (parent line from untreated patients/and derived cisplatin-resistant subline, respectively) were supplied by European Collection of Authenticated Cell Cultures (ECACC, Porton Down Salisbury UK). These cells were maintained in the logarithmic phase at 37 °C under a 5% CO₂ atmosphere and cultured in RPMI 1640 medium supplemented with 10% fetal calf serum, 2 mM glutamine, 10 mg/mL gentamycin and 10 mg/mL insulin. All culture media and reagents were purchased from Euroclone (Sigma-Aldrich, Italy).

2.7. *In vitro* growth inhibition assay

The growth inhibitory effect of compounds was compared to cisplatin (CDPP) by using the sulforhodamine-B (SRB) assay [28]. Briefly, cells were seeded in a 96-well microtiter plates in 100 μ L at plating densities ranging from 2,000 to 12,000 cells/well depending upon the doubling time of individual cell lines. After seeding, microtiter plates were incubated at 37 $^{\circ}$ C, 5% CO₂, 95% air, and 100% relative humidity for 24 h prior to addition of the compounds. After 24 h, samples of each cell line were fixed *in situ* with cold trichloroacetic acid (TCA) to measure the cell population at the time of compound addition. The test compounds were freshly dissolved in dimethyl sulfoxide (DMSO, 10⁻² M) and stepwise diluted to the final maximum test concentration (100 μ M) with complete medium, so that the maximum DMSO/well ratio was 0.25% (v/v). Following the addition of the compound to triplicate wells, the plates were further incubated for 72 h. Cells were fixed *in situ* by the gentle addition of 50 μ L of cold 50% (w/v) TCA (final concentration, 10%) and incubated for 1 h at 4 $^{\circ}$ C. The supernatant was discarded, and the plates were washed four times with tap water and air-dried. Sulforhodamine-B (SRB) solution (100 μ L) at 0.4% (w/v) in 1% acetic acid was added to each well, and plates were incubated for 30 min at room temperature. After staining, unbound dye was removed by washing five times with 1% acetic acid and the plates were air-dried. Bound stain was then solubilized with 10 mM trizma[®] base and the absorbance was read on an automatic plate reader at 570 nm. All the compounds were initially tested at 100 μ M concentration. For compounds showing more than 50% inhibition of cell viability were at 100 μ M, dose-response curves were studied. Five solutions for each compound were prepared (five-fold serial dilution of the 100 μ M solution) and tested in all the cancer cell lines. The compound concentration able to inhibit cell growth by 50% (IC₅₀) was then calculated by nonlinear regression of the semi-logarithmic dose-response plots, using Prisma GraphPad software (vers. 5.01).

2.8. Molecular docking calculation

The chemical structures of compounds **4a**, **4d**, **4f** and **4i** were drawn using ChemDraw pro 12 and further minimized to local energy minima using hybrid based steepest decent till 5000 iterative steps using LBFGS algorithm [36] with default tautomeric and ionized state using EPIK [37].

DNA (PDB ID: 1BNA) was prepared using respective tools of Schrödinger suite of software [29]. The minimization is carried until RMSD cut-off of 0.30 Å for the heavy atoms. Altogether the protonation state and hydrogen bond of the structure are fixed with re-oriented with clash penalty score.

Grid based ligand docking with energetics (GLIDE) [33] was used to find favorable interactions between ligand and the target DNA with flexible conformations of the ligand. Glide scoring function is given by equation below:

$$GScore = 0.05 \times vdW + 0.15 \times Coul + Lipo + Hbond + Reward + RorB + Site + hydrophobicity$$

Glide scoring with XP descriptor with Induced Fit docking (IFD) rewards hydrophobic interactions in-between ligand and the receptors. IFD also reduces false positive of true ligand binder whereby IFD induces side chain flexibility in the receptors [38].

2.9. Fluorescence spectroscopic studies

Calf thymus DNA (ctDNA) was purchased from Sigma Aldrich chemicals & Co. and used without further purification. Ethidium bromide (EtBr, 95% purity) was obtained from Sigma Aldrich. Each test compound (**4d** or **4f**) was initially dissolved in EtOAc and diluted with double distilled water. The emission spectroscopy analysis was

performed using HITACHI F7100 fluorescence spectrophotometer for the ctDNA-EtBr and ctDNA-EtBr with the test compound at 293 K. Initially the excitation wavelength has been set for 530 nm and the emission maximum was observed around 591 nm for free ctDNA (10 μ M)-EtBr (2 μ M) between 550 nm and 800 nm wavelength range. The band pass slit width was set at 5 nm for both excitation and emission. The ctDNA-EtBr concentration was kept constant and compound **4d** (0 to 18 μ M) and **4f** (0 to 20 μ M) were added at 2 μ M intervals. Further, the ctDNA-EtBr with compound **4d** or **4f** complex was studied at three different temperatures (293 K, 297 K and 300 K) using TECAN INFINITE M1000 PRO micro plate reader using the above described procedure. Also, the inner filter effects are reduced for ctDNA-EtBr and test compound complex using Eq. (1):

$$F_{corr} = F_{obs} \cdot e^{(A1+A2)/2} \quad (1)$$

where F_{corr} and F_{obs} represent the fluorescence intensities after and before correction of ctDNA-EtBr with **4d** and **4f** complex at the emission wavelength and $A1$ and $A2$ are the total absorbance of all components at the λ_{ex} and λ_{em} , respectively. The quenching mechanism is determined using Stern-Volmer equation (2)

$$F_0/F = 1 + k_q \tau_0 [PI] = 1 + K_{sv} [PI] \quad (2)$$

where K_{sv} and K_q are quenching constant and rate constant, respectively, whereas F_0 and F are the emission intensity in the absence and presence of the test compound, respectively, in ctDNA-EtBr; τ_0 is the life time of ctDNA-EtBr. The double logarithmic calculation was performed using Eq. (3), to calculate the binding constant and binding stability of compounds **4d** and **4f** in ctDNA-EtBr system:

$$\text{Log}[(F_0-F)/F] = \text{Log}K_b + n \text{log}[\text{compound}] \quad (3)$$

where K_b is the binding constant and n is the various binding sites in ctDNA-EtBr binding site.

According to Ross, Subramanian et al. [31], the thermodynamic parameters enthalpy (ΔH°), entropy (ΔS°) and binding free energy (ΔG°) were calculated for compound **4d** and **4f** in ctDNA-EtBr complex system using van't Hoff Eqs. (4) and (5).

$$\text{Log} K_b = -\frac{\Delta H^{\circ}}{2.303 RT} + \frac{\Delta S^{\circ}}{2.303 R} \quad (4)$$

$$\Delta G^{\circ} = \Delta H^{\circ} - T \Delta S^{\circ} = -RT \ln K_b \quad (5)$$

where R is the gas constant.

3. Conclusions

A novel preparative protocol has been developed which allows the synthesis of chromeno[2,3-*c*]isoquinoline-5-amine analogs to be achieved in a single step reaction with moderate-to-good yields. The preparation relies on an effective domino reaction, consecutively involving a Knoevenagel condensation, two nucleophilic cyclizations and a reduction step. The synthesized polycyclic derivatives showed antiproliferative activities against some human tumor cells, namely breast (MCF-7), colon (HCT116) and ovarian carcinoma (A2780) cell lines, including cisplatin-resistant ovarian cancer cells (SK-OV-3 and A2780cp8), with IC₅₀s in the low micromolar range (< 10 μ M). While further target validation and mechanistic studies are expected to support the structure-based drug design of new more potent analogs, the SAR study highlights the favorable effects of small alkoxy groups (methoxy, ethoxy) in C8 and C10 of the chromeno[2,3-*c*]isoquinoline scaffold, leading to compounds **4d** and **4f** which should be noteworthy for the future optimization studies. Molecular docking calculation results, experimentally confirmed by fluorescence quenching studies, suggest the binding of DNA with the typical features of the most common intercalating ligands as a possible mechanism underlying the antiproliferative activity of the chromeno[2,3-*c*]isoquinoline-5-amines investigated herein.

Declaration of Competing Interest

The authors declare that they have no known competing financial interests or personal relationships that could have appeared to influence the work reported in this paper.

Acknowledgements

The synthetic part of the work has been funded by the Russian Science Foundation (project № 18-73-00017). The computational part of the work was prepared with the support of the “RUDN University Program 5-100”. The Italian authors A.B, R.P. and C.D.A. acknowledge the financial support of the Italian Ministry of Education, Universities and Research (PRIN, Grant 201744BN5T_004).

Appendix A. Supplementary data

Supplementary data to this article can be found online at <https://doi.org/10.1016/j.bioorg.2020.104169>.

References

- L.F. Tietze, *Domino Reactions: Concepts for efficient organic synthesis*, Wiley-VCH Verlag GmbH & Co. KGaA, Weinheim, Germany, 2014. Doi: [10.1002/9783527671304](https://doi.org/10.1002/9783527671304).
- S.A. Snyder, *Applications of Domino Transformations in Organic Synthesis 2*, Georg Thieme Verlag, Stuttgart, 2016. Doi: [10.1055/b-003-128260](https://doi.org/10.1055/b-003-128260).
- M.J. Oset-Gasque, M.P. González, J. Pérez-Peña, N. García-Font, A. Romero, J. Del Pino, E. Ramos, D. Hadjipavlou-Litina, E. Soriano, M. Chioua, A. Samadi, D.S. Raghuvanshi, K.N. Singh, J. Marco-Contelles, Toxicological and pharmacological evaluation, antioxidant, ADMET and molecular modeling of selected racemic chromenotacrine 11-amino-12-aryl-8,9, 10,12-tetrahydro-7H-chromeno[2,3-b]quinolin-3-ols for the potential prevention and treatment of Alzheimer's, *Eur. J. Med. Chem.* 74 (2014) 491–501, <https://doi.org/10.1016/j.ejmech.2013.12.021>.
- H. Makino, T. Saijo, Y. Ashida, H. Kuriki, Y. Maki, Mechanism of action of an anti-allergic agent, Amlexanox (AA-673), in inhibiting histamine release from mast cells, *Int. Arch. Allergy Immunol.* 82 (1987) 66–71, <https://doi.org/10.1159/000234292>.
- I. Akyol-Salman, D. Leçe-Sertöz, O. Baykal, Topical pranopfen 0.1% is as effective anti-inflammatory and analgesic agent as diclofenac sodium 0.1% after strabismus surgery, *J. Ocul. Pharmacol. Ther.* 23 (2007) 280–283, <https://doi.org/10.1089/jop.2006.108>.
- Y. Liu, J. Lu, Z. Zhang, L. Zhu, S. Dong, G. Guo, R. Li, Y. Nan, K. Yu, Y. Zhong, Q. Huang, Amlexanox, a selective inhibitor of IKKε, generates anti-tumoral effects by disrupting the Hippo pathway in human glioblastoma cell lines, *Cell Death Dis.* 8 (2017) e3022, <https://doi.org/10.1038/cddis.2017.396>.
- S.M. Reilly, S. Chiang, S.J. Decker, L. Chang, M.J. Larsen, J.R. Rubin, J. Mowers, N.M. White, M. Downes, R. Yu, C. Liddle, R.M. Evans, P. Li, J.M. Olefsky, A.R. Saltiel, An inhibitor of the protein kinases TBK1/IKKε improves obesity-related metabolic dysfunctions, *Nat. Med.* 19 (2013) 313–321, <https://doi.org/10.1038/nm.3082>.
- T.S. Beyett, X. Gan, S.M. Reilly, L. Chang, A.V. Gomez, A.R. Saltiel, H.D. Showalter, J.J.G. Tesmer, Carboxylic acid derivatives of amlexanox display enhanced potency toward TBK1 and IKKε and reveal mechanisms for selective inhibition, *Mol. Pharmacol.* 94 (2018) 1210–1219, <https://doi.org/10.1124/mol.118.112185>.
- T.S. Beyett, X. Gan, S.M. Reilly, A.V. Gomez, L. Chang, J.J.G. Tesmer, A.R. Saltiel, H.D. Showalter, Design, synthesis, and biological activity of substituted 2-amino-5-oxo-5H-chromeno[2,3-b]pyridine-3-carboxylic acid derivatives as inhibitors of the inflammatory kinases TBK1 and IKKε for the treatment of obesity, *Bioorganic Med. Chem.* 26 (2018) 5443–5461, <https://doi.org/10.1016/j.bmc.2018.09.020>.
- S.K. Halder, H. Ueda, Amlexanox inhibits cerebral ischemia-induced delayed astrocytic high-mobility group box 1 release and subsequent brain damage, *J. Pharmacol. Exp. Ther.* 365 (2018) 27–36, <https://doi.org/10.1124/jpet.117.245340>.
- C.F. Lima, M. Costa, M.F. Proença, C. Pereira-Wilson, Novel structurally similar chromene derivatives with opposing effects on p53 and apoptosis mechanisms in colorectal HCT116 cancer cells, *Eur. J. Pharm. Sci.* 72 (2015) 34–45, <https://doi.org/10.1016/j.ejps.2015.02.019>.
- W. Zhang, J. Wang, J. Mao, L. Hu, X. Wu, C. Guo, Three-component domino cyclization of novel carbazole and indole fused pyrano[2,3-c]pyridine derivatives, *Tetrahedron Lett.* 57 (2016) 1985–1989, <https://doi.org/10.1016/j.tetlet.2016.03.081>.
- A.N. Vereshchagin, M.N. Elinson, Y.E. Anisina, F.V. Ryzhkov, R.A. Novikov, M.P. Egorov, PASE pseudo-four-component synthesis and docking studies of new 5-c-substituted 2,4-diamino-5H-chromeno[2,3-b]pyridine-3-carbonitriles, *ChemistrySelect.* 2 (2017) 4593–4597, <https://doi.org/10.1002/slct.201700606>.
- S.-T. Chung, W.-H. Huang, C.-K. Huang, F.-C. Liu, R.-Y. Huang, C.-C. Wu, A.-R. Lee, Synthesis and anti-inflammatory activities of 4H-chromene and chromeno[2,3-b]pyridine derivatives, *Res. Chem. Intermed.* 42 (2016) 1195–1215, <https://doi.org/10.1007/s11164-015-2081-7>.
- A.N. Vereshchagin, M.N. Elinson, Y.E. Anisina, F.V. Ryzhkov, A.S. Goloveshkin, M.P. Egorov, Synthesis, structural, spectroscopic and docking studies of new 5C-substituted 2,4-diamino-5H-chromeno[2,3-b]pyridine-3-carbonitriles, *J. Mol. Struct.* 1146 (2017) 766–772, <https://doi.org/10.1016/j.molstruc.2017.06.044>.
- K.A. Grice, R. Patil, A. Ghosh, J.D. Paner, M.A. Guerrero, E.J.M. Camacho, P. Sun Cao, A.H. Niyazi, S. Zainab, R.D. Sommer, G. Waris, S. Patil, Understanding the structure and reactivity of the C-S linkage in biologically active 5-arylthio-5H-chromenopyridines, *New J. Chem.* 42 (2018) 1151–1158, <https://doi.org/10.1039/C7NJ03724D>.
- M.N. Elinson, A.N. Vereshchagin, Y.E. Anisina, A.N. Fakhruddinov, A.S. Goloveshkin, M.P. Egorov, Pot-, Atom- and Step-Economic (PASE) Multicomponent Approach to the 5-(Dialkylphosphonate)-Substituted 2,4-Diamino-5H-chromeno[2,3-b]pyridine Scaffold, *European J. Org. Chem.* 2019 (2019) 4171–4178, <https://doi.org/10.1002/ejoc.201900240>.
- A.A. Festa, O.A. Storozhenko, D.R. Bella Ndoutoume, A.V. Varlamov, L.G. Voskressensky, Sequential three-component reaction of homophthalonitrile, salicylaldehydes and nitromethane, *Mendeleev Commun.* 27 (2017) 451–453, <https://doi.org/10.1016/j.mencom.2017.09.006>.
- A.A. Festa, O.A. Storozhenko, N.E. Golantsov, K. Subramani, R.A. Novikov, S.O. Zaitseva, M.S. Baranov, A.V. Varlamov, L.G. Voskressensky, Homophthalonitrile for multicomponent reactions: syntheses and optical properties of o-cyanophenyl- or indol-3-yl-substituted chromeno[2,3-c]isoquinolin-5-amines, *ChemistryOpen.* 8 (2019) 23–30, <https://doi.org/10.1002/open.201800207>.
- L.G. Voskressensky, E.A. Sokolova, A.A. Festa, A.V. Varlamov, A novel domino condensation-intramolecular nucleophilic cyclization approach towards annulated thiochromenes, *Tetrahedron Lett.* 54 (2013) 5172–5173, <https://doi.org/10.1016/j.tetlet.2013.07.040>.
- L.G. Voskressensky, O.A. Storozhenko, A.A. Festa, R.A. Novikov, A.V. Varlamov, Synthesis of chromenoimidazoles annulated with an azaindole moiety, through a base-promoted domino reaction of cyano methyl quaternary salts, *Synth.* 49 (2017) 2753–2760, <https://doi.org/10.1055/s-0036-1589496>.
- O.A. Storozhenko, A.A. Festa, D.R.B. Ndoutoume, A.V. Aksenov, A.V. Varlamov, L.G. Voskressensky, Mn-mediated sequential three-component domino Knoevenagel/cyclization/Michael addition/oxidative cyclization reaction towards annulated imidazo[1,2-a]pyridines, *Beilstein J. Org. Chem.* 14 (2018) 3078–3087, <https://doi.org/10.3762/bjoc.14.287>.
- E.A. Sokolova, A.A. Festa, N.E. Golantsov, N.S. Lukonina, I.N. Ioffe, A.V. Varlamov, L.G. Voskressensky, Highly fluorescent pyrido[2,3-b]indolizine-10-carbonitriles through pseudo three-component reactions of N-(Cyanomethyl)pyridinium salts, *Eur. J. Org. Chem.* 2019 (2019) 6770–6775, <https://doi.org/10.1002/ejoc.201900995>.
- A.A. Festa, N.E. Golantsov, O.A. Storozhenko, A.N. Shumsky, A.V. Varlamov, L.G. Voskressensky, Alcohol-initiated dinitrile cyclization in basic media: a route toward pyrazino[1,2-a]indole-3-amines, *Synlett.* 29 (2018) 898–903, <https://doi.org/10.1055/s-0036-1591529>.
- M.D. Matveeva, R. Purgatorio, L.G. Voskressensky, C.D. Altomare, Pyrrolo[2,1-a]isoquinoline scaffold in drug discovery: advances in synthesis and medicinal chemistry, *Fut. Med. Chem.* 11 (2019) 2735–2755, <https://doi.org/10.4155/fmc-2019-0136>.
- A.A. Nevskaya, M.D. Matveeva, T.N. Borisova, M. Niso, N.A. Colabufo, A. Boccarelli, R. Purgatorio, M. de Candia, S. Cellamare, L.G. Voskressensky, C.D. Altomare, A new class of 1-aryl-5,6-dihydropyrrolo[2,1-a]isoquinoline derivatives as reversers of P-glycoprotein-mediated multidrug resistance in tumor cells, *Fut. Med. Chem.* 13 (2018) 1588–1596, <https://doi.org/10.1002/cmdc.201800177>.
- K. Bhadra, G.S. Kumar, Isoquinoline alkaloids and their binding with DNA: calorimetry and thermal analysis applications, *Mini Rev. Med. Chem.* 10 (2010) 1235–1247, <https://doi.org/10.2174/13895575110091235>.
- P. Skehan, R. Storeng, D. Scudiero, A. Monks, J. McMahon, D. Vistica, J.T. Warren, H. Bokesch, S. Kenney, M.R. Boyd, New colorimetric cytotoxicity assay for anticancer-drug screening, *J. Natl. Cancer Inst.* 82 (1990) 1107–1112, <https://doi.org/10.1093/jnci/82.13.1107>.
- B.C. Behrens, T.C. Hamilton, H. Masuda, K.R. Grotzinger, J. Whang-Peng, K.G. Louie, T. Knutsen, W.M. Mckoy, R.C. Young, R.F. Ozols, Characterization of a cis-diamminedichloroplatinum(II)-resistant human ovarian cancer cell line and its use in evaluation of platinum analogues, *Cancer Res.* 47 (1987) 414–418.
- M. Coluccia, A. Nassi, A. Boccarelli, D. Giordano, N. Cardellicchio, F.P. Intini, G. Natile, A. Barletta, A. Paradiso, In vitro antitumor activity and cellular pharmacological properties of the platinum-iminoether complex trans-[PtCl₂(E)-HN=C(Ome)Me]₂, *Int. J. Oncol.* 15 (1999) 1039–1044, <https://doi.org/10.3892/ijo.15.5.1039>.
- Y. Gilad, H. Sendorowitz, Docking studies on DNA intercalators, *J. Chem. Inf. Model.* 54 (2014) 96–107.
- C. De Ford, K. Penchalaiah, A. Krefit, M. Humar, W. Heydenreuter, M. Kangan, S.A. Sieber, L.F. Tietze, I. Merfort, Bifunctional duocarmycin analogues as inhibitors of protein tyrosine kinases, *J. Nat. Prod.* 82 (2019) 16–26.
- Glide, Schrödinger, LCC, Schrödinger Release 2018-2, (2019).
- S. Karthikeyan, R.R. Zalte, A.A. Festa, L.G. Voskressensky, Understanding the binding mechanism of a pyrazino[1,2-a]indole derivative with calf thymus DNA,

- ChemistrySelect. 4 (2019) 5214–5221, <https://doi.org/10.1002/slct.201803838>.
- [35] P.D. Ross, S. Subramanian, Thermodynamics of protein association reactions: forces contributing to stability, *Biochemistry*. 20 (1981) 3096–3102, <https://doi.org/10.1021/bi00514a017>.
- [36] J.C. Shelley, A. Cholleti, L.L. Frye, J.R. Greenwood, M.R. Timlin, M. Uchimaya, Epik: a software program for pK_a prediction and protonation state generation for drug-like molecules, *J. Comput. Aided. Mol. Des.* 21 (2007) 681–691, <https://doi.org/10.1007/s10822-007-9133-z>.
- [37] J.R. Greenwood, D. Calkins, A.P. Sullivan, J.C. Shelley, Towards the comprehensive, rapid, and accurate prediction of the favorable tautomeric states of drug-like molecules in aqueous solution, *J. Comput. Aided. Mol. Des.* 24 (2010) 591–604, <https://doi.org/10.1007/s10822-010-9349-1>.
- [38] W. Sherman, H.S. Beard, R. Farid, Use of an induced fit receptor structure in virtual screening, *Chem. Biol. Drug Des.* 67 (2006) 83–84, <https://doi.org/10.1111/j.1747-0285.2005.00327.x>.